Surface Integrity Evolution in WEDM of Nickel-Based Superalloys: Formation and Implications of Recast Layer, Residual Stresses, and Microhardness—A Critical Review

Gurnam Singh *, Neel Kanth Grover and Vivek Aggarwal
Department of Mechanical Engineering, IK Gujral Punjab Technical University, Kapurthala, Punjab, 144603, India
***Corresponding Author E-mail:** gurnamsingh@sbsstc.ac.in
Received: May 17, 2026; **Revised:** Aug 06, 2026; **Accepted:** Aug 07, 2026

Abstract

Wire Electrical Discharge Machining (WEDM) is widely applied for machining nickel-based superalloys used in aerospace and high-temperature systems; however, thermally induced surface alterations strongly affect structural reliability. This review synthesizes recast layer thickness (RLT), microhardness evolution, residual stress development, and elemental redistribution in precipitation- and solid-solution-strengthened alloys. Discharge energy—mainly governed by pulse-on time and peak current and influenced by gap voltage—controls melt-pool behavior, resolidification, chemical modification, and stress evolution. Reported RLT values vary from ~1 to 50 µm depending on machining regime, while low-energy multi-trim strategies can restrict thickness below ~5–6 µm for aerospace requirements. High discharge energy promotes Cu–Zn electrode transfer, oxygen incorporation, and tensile residual stresses (~200–800 MPa), increasing crack susceptibility. Microhardness response is alloy-dependent, often showing subsurface softening under aggressive conditions. This review establishes an energy–microstructure–performance framework for improving surface integrity in critical applications.

Keywords: WEDM, Nickel-based superalloys, Recast layer, Surface integrity, Residual stress, Microhardness

1. Introduction

Nickel-based superalloys are extensively utilized in aerospace, nuclear, and chemical industries owing to their exceptional strength, corrosion resistance, and microstructural stability at elevated temperatures. They maintain mechanical integrity under severe thermo-mechanical loading and exhibit excellent resistance to oxidation, creep, and fatigue. Consequently, these alloys constitute more than 50% of the materials used in modern aerospace engines, particularly in gas turbine hot-section components such as turbine disks, blades, vanes, combustors, and casings. Their durability in aggressive environments further supports their application in nuclear and chemical processing systems. However, their high strength, pronounced work-hardening tendency, and low thermal conductivity severely restrict conventional machinability, necessitating advanced non-conventional machining techniques for precision manufacturing [1].

Electrical Discharge Machining (EDM) is widely employed for machining such difficult-to-cut materials, although it significantly influences surface integrity. During each discharge, localized melting and partial vaporization occur, followed by rapid resolidification of residual molten material, forming a recast layer. Beneath this layer, a heat-affected zone (HAZ) develops, often characterized by microstructural transformations, tensile residual stresses, microcracks, and elemental redistribution, which may impair fatigue and corrosion performance [2].

The superior high-temperature capability of nickel-based superalloys arises from synergistic solid-solution strengthening (via elements such as Mo, W, Re, and Co) and precipitation hardening through coherent γ′ ($Ni_3(Al,Ti)$) and γ″ phases that effectively hinder dislocation motion. Their nickel-rich FCC matrix, alloyed with Cr, Al, Ti, Nb, W, and Mo, provides an optimal balance between strength and ductility at elevated temperatures. Accordingly, alloy families such as Inconel, René, Waspaloy, Udimet, Nimonic, and Hastelloy are extensively employed in critical high-temperature applications [3–5].

Recent research has increasingly focused on understanding surface integrity modifications induced by Wire Electrical Discharge Machining (WEDM) in nickel-based superalloys. Although the fundamental spark-erosion mechanism remains similar across materials [6], alloy-specific composition, precipitation-strengthening phases, and thermophysical properties significantly influence recast layer formation, defect evolution, and microhardness distribution [7]. In addition to morphological changes, intense thermo-electrical cycles during WEDM promote electrode-derived elemental redistribution and oxygen incorporation within the resolidified layer, thereby altering local surface chemistry. Simultaneously, rapid heating and quenching generate steep thermal gradients that lead to the development of residual stress fields within the recast layer and the underlying heat-affected zone. These coupled microstructural, chemical, and mechanical modifications vary considerably among different nickel-based superalloys [6],7]. Therefore, a systematic comparative review of WEDM-induced recast layer characteristics, microhardness evolution, residual stress development, and elemental

redistribution across various superalloys is essential for identifying material-dependent trends and establishing a comprehensive understanding of surface integrity responses.

2. Methodology and Literature Search Strategy

To ensure scientific rigor, objectivity, and reproducibility, literature selection for this systematic review was conducted following the Preferred Reporting Items for Systematic Reviews and Meta-Analyses (PRISMA) guidelines. A comprehensive bibliographic search was executed across major indexing databases, including Web of Science, Scopus, ScienceDirect, and Google Scholar, covering peer-reviewed articles published up to 2026.

2.1 Search Keywords and Boolean Operators

To capture all relevant peer-reviewed studies on wire spark erosion processes, the literature search utilized combinations of primary keywords and Boolean operators:

- ("Wire Electrical Discharge Machining" OR "WEDM" OR "EDWC" OR "Electric Discharge Wire Cutting") AND
- ("Nickel-based Superalloys" OR "Inconel" OR "Nimonic" OR "Udimet" OR "NiTi") AND
- ("Surface Integrity" OR "Recast Layer Thickness" OR "Microhardness" OR "Elemental Redistribution" OR "Surface Crack Density").

2.2 Inclusion and Exclusion Criteria

Studies were evaluated against predefined eligibility criteria:

- **Inclusion Criteria:** (i) Peer-reviewed original research articles evaluating WEDM or EDWC of nickel-based superalloys or Ni-rich shape memory alloys; (ii) Quantitative reporting of surface integrity parameters, specifically recast layer thickness (RLT), surface crack density (SCD), microhardness profiles, or elemental migration via SEM, EDX, or XRD; (iii) Studies providing clear experimental discharge conditions (e.g., pulse duration, peak current, discharge energy).
- **Exclusion Criteria:** (i) Studies evaluating conventional die-sinking electrical discharge machining (EDM) or non-wire hybrid processes (to maintain exclusive focus on wire electrical discharge machining); (ii) non-English publications; (iii) Articles lacking explicit experimental validation or quantifiable surface integrity data.

2.3 Screening and Selection Pipeline

As illustrated in the systematic PRISMA flowchart (**Figure 1**), the search strategy initially identified 315 records across the target databases. After removing 87 duplicate entries, 228 unique records underwent title and abstract screening, leading to the exclusion of 112 studies that did not meet the primary scope. A full-text evaluation of the remaining 116 articles was conducted, resulting in the exclusion of 50 studies due to insufficient surface integrity data, non-wire process configurations, or non-relevant alloy chemistry. Ultimately, 66 high-impact research papers met all eligibility criteria and were synthesized in this review [8],[9].

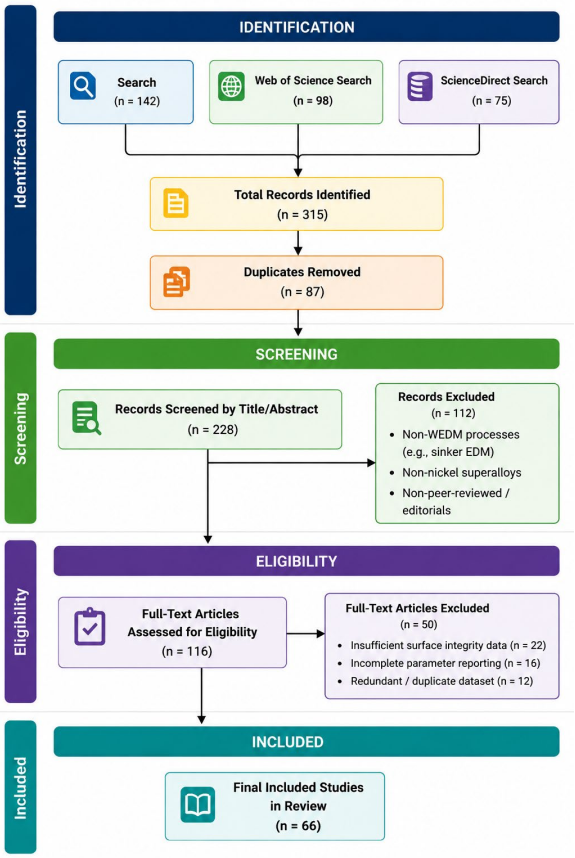


Figure 1 Systematic PRISMA flowchart illustrating the identification, screening, eligibility, and selection process of literature on wire electrical discharge machining of nickel-based superalloys.

3. Critical Synthesis of Characterization Methodologies and Measurement Principles

Evaluating WEDM-induced surface degradation in nickel-based superalloys requires understanding the physical mechanics, resolution constraints, and sampling uncertainties of key analytical techniques.

3.1 X-Ray Diffraction (XRD): Residual Stress & Phase Analysis

Residual stress profiling relies on the $\sin^2\psi$ technique, where macro-tensile stresses from dielectric quenching alter interplanar spacing (d), producing measurable 2θ peak shifts according to Bragg's Law ($n\lambda = 2d\sin\theta$) [10],[11]. Peak broadening (FWHM analysis via Scherrer or Williamson–Hall equations) additionally quantifies sub-grain crystallite refinement and micro-strain [10]. However, standard laboratory XRD (Cu-Kα/Cr-Kα) penetrates 5–15 μm If the recast layer is thinner than this sampling depth, the diffracted signal averages the tensile recast layer with the underlying matrix,

necessitating chemical polishing, grazing-incidence techniques, or advanced method comparisons for true depth-resolved profiling [11],[12].

3.2 Vickers Microhardness Profiling across the Subsurface

Vickers microhardness testing ($HV = 1.8544 \cdot P/d^2$) maps thermal softening in the heat-affected zone (HAZ) and hardening in the recast layer on cross-sections as per ASTM E384 [13]. According to ASTM guidelines, indentation spacing and edge distances must exceed 2.5× the diagonal length (d) to prevent edge deflection and plastic zone overlap [13]. Consequently, heavy loads > 100g blur thin recast boundaries (<15 μm) by measuring composite responses, whereas light loads (10–25g) enable fine spatial resolution (5–10 μm steps) but introduce the Indentation Size Effect (ISE).

3.3 Energy Dispersive X-Ray Spectroscopy (EDS/EDX): Elemental Redistribution

EDS quantifies tool-wire material migration (Cu--Zn diffusion), dielectric decomposition products (C and O ingress), and non-uniform alloying element segregation (Nb, Ti, Mo, Cr) driven by rapid thermal solidification during Wire EDM machining [14]. Sample size and preparation are critical: small excised cross-sectional coupons (10 × 10 mm) must be mounted in conductive media with edge-retention resins to prevent edge-rounding, ensuring the recast boundary remains flat. Accelerating voltages (15–20kV) produce an excitation interaction volume extending 1–2 μm deep, which can penetrate beyond ultra-thin recast layers during surface-normal scanning [14]. Consequently, cross-sectional line profiles and area mapping are required. Quantitative EDS also suffers from severe absorption errors for light elements (Z < 11, e.g., C and O), requiring Wavelength Dispersive Spectroscopy (WDS) or XPS for precise chemical state verification [14].

3.4 Scanning Electron Microscopy (SEM): Topography & Layer Boundaries

SEM provides high-resolution imaging of discharge craters, recast layer uniformity, and subsurface micro-cracks on metallographic cross-sections (10 × 10 mm specimens) [14]. Differentiating signal modes is crucial: Secondary Electron (SE) mode provides topographic contrast of surface debris and cracks, whereas Backscattered Electron (BSE) mode yields atomic number (Z) contrast [14]. Because element diffusion from the wire and phase segregation alter the recast layer's chemical composition, BSE mode provides a distinct compositional boundary against the parent superalloy, minimizing measurement error during recast layer thickness (RLT) quantification [14].

3.5 EBSD & TEM: Nanostructural, Strain, & Precipitate Dynamics

Advanced electron diffraction techniques resolve subsurface phenomena beyond optical and conventional SEM limits:

- Electron Backscatter Diffraction (EBSD): Maps rapid solidification structures (columnar-to-equiaxed transitions) and crystallographic orientation on flat, damage-free polished samples. High-resolution transmission EBSD (t-EBSD) enables fine mapping of localized plastic strain, dislocation density, and microstructural orientation across ultrafine subsurface zones [15].
- Transmission Electron Microscopy (TEM): Isolates atomic-scale transformations within FIB-prepared foils (~100 nm thick, excised from 3 mm TEM discs or site-specific surface locations). Orientation and phase mapping in TEM (EBSD-like diffraction) reveal grain refinement, amorphous layer boundaries, and precipitate dynamics—specifically the thermal dissolution and over-aging of strengthening γ' ($Ni_3(Al, Ti)$) and γ'' (Ni_3Nb) phases exposed to peak spark temperatures (> 10,000 K) [16].

4. Literature Review

A substantial body of research has examined surface integrity during WEDM of nickel-based superalloys; however, much of the literature remains parameter-centric rather than mechanism-oriented. While machining performance indicators such as material removal rate and surface roughness are extensively reported, comparatively fewer studies provide integrated assessments of recast layer evolution, hardness gradients, residual stress development, and compositional modification under comparable discharge conditions. The following thematic analysis critically synthesizes existing contributions.

4.1 Definition and Benchmarks of Surface Integrity

In WEDM of nickel-based superalloys, surface integrity refers to the topographical (Ra, Rz, craters), metallurgical (recast layer, HAZ, γ′/γ″ phase dissolution), chemical (Cu–Zn wire transfer, C/O ingress, element segregation), and mechanical (residual stress, microhardness) condition of the surface and immediate subsurface (0–100 μm).

For mission-critical aerospace and energy components, “good” (optimal) surface integrity is defined as a state that maximizes fatigue life and structural reliability [17],[18]. Specifically, this requires:

- Minimal Recast Layer & Zero Micro-cracks: Complete suppression or thinning (< 2 μm) of the recast layer without micro-crack propagation into the parent alloy [18],[19].
- Compressive Subsurface Stress: Low tensile surface stresses transitioning rapidly to deep compressive residual stresses [18].
- Metallurgical Homogeneity: Retained base-alloy stoichiometry with minimal wire material contamination or element segregation [18],[19].
- Low Surface Roughness: Smooth finish (Ra < 0.4 μm) to minimize stress concentration factors (Kt) [18],[19].

To systematically evaluate how WEDM operational parameters govern these surface integrity benchmarks, the following subsections examine the fundamental drivers of thermal degradation, starting with the primary tool interface.

4.2 Influence of Wire Electrode Characteristics in WEDM

Wire characteristics, including electrode material, diameter, and coating composition, significantly influence discharge stability and the thermo–electrical interaction between the wire electrode and the workpiece during WEDM. These parameters affect spark initiation, energy distribution, and debris evacuation, thereby controlling recast layer formation, microhardness gradients, and residual stress development within the machined surface. Antar et al. [20] demonstrated that Zn-coated copper-core wires enhance dielectric ionization and debris flushing efficiency during machining of Udimet 720, resulting in reduced recast layer thickness, lower crack density, and decreased tensile residual stresses in the resolidified layer. Reolon et al. [21] reported similar improvements for Inconel 718, where coated wires produced more uniform discharges and mitigated localized stress concentrations within the recast layer. In addition to coating composition, wire diameter and material properties also affect the magnitude of thermal energy transferred to the workpiece. Sharma et al. [22],[23] showed that variations in wire material and diameter altered recast layer thickness, subsurface hardness gradients, and residual stress distribution in Inconel 706. Larger wire diameters were associated with increased spark energy and thicker recast layers, whereas coated wires improved machining stability and surface integrity. Despite these findings, systematic comparative studies evaluating wire electrode characteristics across different nickel-based superalloys under identical discharge-energy conditions remain limited.

4.3 Influence of Discharge Energy and Process Parameters

Discharge energy—primarily governed by pulse-on time, peak current, and gap voltage—consistently emerges as the dominant parameter controlling surface integrity during WEDM. Higher discharge energy intensifies thermal penetration and melt pool formation, producing thicker recast layers, increased elemental redistribution, and elevated tensile residual stresses at the machined surface. Li et al. [24] demonstrated that trim-cut strategies effectively reduce white-layer thickness and associated residual stress concentration in Inconel 718, highlighting the importance of controlled low-energy regimes. Atzeni et al. [25] further proposed the concept of nominal discharge energy per unit length as a unified descriptor of machining conditions, enabling improved correlation between process parameters and surface integrity characteristics. Abhilash and Chakradhar [26] emphasized the role of machining stability and inter-electrode gap control, reporting that unstable discharge conditions significantly exacerbate recast layer growth, compositional contamination, and stress accumulation. Similar energy-dependent behavior has been reported for several nickel-based superalloys, including Nimonic 80A [27],[28], Nimonic 90 [29], Inconel 738 [30], and MONEL K-500 [31]. Despite the consistent identification of discharge energy as the dominant governing factor, most investigations analyze individual alloys independently, limiting the development of generalized energy–microstructure–property–stress relationships applicable across multiple superalloy systems.

4.4 Surface Integrity and Mechanical Performance

Only a limited number of investigations have directly correlated WEDM-induced surface integrity characteristics with mechanical performance in nickel-based superalloys. Chen et al. [32] demonstrated that surface defects and tensile residual stresses generated during WEDM of Inconel 718 play a critical role in fatigue crack initiation and propagation. Their results showed that micro-cracks, recast layer porosity, and residual stress concentration significantly reduce fatigue life, indicating that surface integrity assessment cannot rely solely on surface roughness measurements. Similarly, Shabgard et al. [33] reported crack formation, hardness variation, and tensile residual stress development in WEDM-processed Inconel 617, highlighting the vulnerability of thermally affected layers to structural degradation. Alkahlan et al. [34] further provided detailed microstructural and micromechanical characterization of the resolidified layer using advanced analytical techniques, revealing heterogeneous mechanical behavior within the recast layer accompanied by complex residual stress distributions. These findings demonstrate that the combined influence of recast layer morphology, hardness gradients, and residual stress fields significantly affects fatigue resistance, crack susceptibility, and long-term structural reliability. However, such comprehensive mechanistic studies remain relatively scarce and are largely concentrated on a few widely studied alloys, particularly Inconel 718.

4.5 Alloy-Specific Surface Integrity Studies

Several investigations have examined WEDM-induced surface integrity behavior in specific nickel-based superalloys, revealing significant material-dependent responses. Sharma et al. [22],[23],[35],[36] conducted systematic studies on Inconel 706, demonstrating that discharge energy, wire characteristics, and process optimization strongly influence recast layer thickness, subsurface hardness gradients, and residual stress distribution. Mouralová et al. [37] investigated WEDM of B1914 alloy and reported distinct recast layer morphology and elemental diffusion behavior, emphasizing the role of alloy composition and solidification characteristics in determining surface modification patterns. Similar studies on Udimet-L605 [38], Nimonic C-263 [39],[40], Inconel 690 [41], Hastelloy X [42], and

Waspaloy [43] have confirmed that precipitation mechanisms, alloy chemistry, and thermophysical properties significantly influence recast layer formation, crack development, and microhardness evolution. Despite these insights, cross-alloy comparisons remain limited due to differences in experimental conditions and parameter selection across studies, making it difficult to establish generalized relationships between WEDM parameters and surface integrity responses.

4.6 Additively Manufactured and Advanced Alloys

Recent research has increasingly extended WEDM investigations to additively manufactured (AM) nickel-based superalloys and advanced functional materials. Ozaner et al. [44] and Karthikeyan et al. [45] reported that the anisotropic microstructure and heterogeneous grain morphology inherent to AM superalloys significantly influence recast layer formation, subsurface hardness distribution, and residual stress development during WEDM. In these materials, the presence of elongated columnar grains, interdendritic solute segregation zones, and pronounced crystallographic textures alters localized heat dissipation and resolidification dynamics compared with conventionally wrought or cast alloys. To highlight the fundamental differences between additive and conventional states, comparative studies on laser powder bed fusion (LPBF) structures—including benchmark austenitic alloys such as AISI 316L studied by Machno et al. [46]—demonstrate that altered pore distribution and grain boundary density in LPBF materials alter localized melting efficiency and subsurface heat accumulation during WEDM. Consequently, LPBF components require tighter regulation of pulse energy (T_{on} and T_{off}) and flushing dynamics to mitigate deep thermal damage and excessive recast layer growth compared to their cast counterparts.

Crucially, the unique microstructural features produced by laser-based additive manufacturing—such as sub-micron cellular networks, high dislocation densities, and dense grain boundary networks—directly govern spark erosion behavior and discharge gap stability in nickel superalloys. As highlighted by Gokcekaya et al. [47] in their investigation of LPBF Inconel 718, these grain boundary configurations and orientation-dependent thermal/electrical conductivities induce transient discharge pulse fluctuations during WEDM. These discharge instabilities lead to uneven energy distribution across the plasma channel, directly causing localized variations in recast layer thickness, heightened microcracks along grain boundaries, and complex tensile-to-compressive residual stress gradients within the heat-affected zone (HAZ).

Similar surface integrity issues have been identified in NiTi-based shape memory alloys [48],[49], where extreme compositional sensitivity and stress-induced phase transformations amplify elemental redistribution, phase instability, and micro-crack propagation inside the resolidified zone. Collectively, these studies confirm that initial microstructural orientation, phase distribution, and thermophysical anisotropy in advanced additive alloys serve as primary governing factors in dictating WEDM-induced surface modification mechanisms and downstream fatigue performance.

4.7 Existing Reviews and Research Gaps

Several review studies [50–54] have summarized the influence of WEDM parameters on machining performance and surface morphology of nickel-based superalloys, consistently reporting that pulse-on time, peak current, and gap voltage govern primary machining responses. To resolve complex conflicting response interactions among these parameters, recent research has transitioned toward hybrid metaheuristic frameworks; notably, Joshi et al. [55] integrated TOPSIS with Multi-Objective Ant-Lion Optimization to identify Pareto-optimal baseline settings for Inconel 718. However, most existing literature primarily emphasizes productivity metrics such as material removal rate and surface roughness, while systematic cross-alloy comparisons addressing integrated surface integrity mechanisms—including recast layer thickness, microhardness evolution, residual stress distribution, and elemental redistribution—remain limited. Consequently, the recast layer must be viewed not merely as a byproduct of spark erosion, but as a thermodynamically driven microstructural transformation controlled by transient thermal gradients, flushing efficiency, and resolidification kinetics. Moreover, while offline optimization models establish static baseline settings, a critical research gap remains in developing real-time closed-loop pulse energy adaptation; existing commercial controllers adjust parameters to prevent wire breakage rather than utilizing in-situ feedback to dynamically suppress subsurface thermal damage, recast layer spikes, and micro-cracking during complex superalloy cuts. A comprehensive understanding of these interconnected mechanisms is therefore necessary to establish a unified framework describing WEDM-induced surface integrity behavior in nickel-based superalloys.

Figure 2 illustrates the conceptual relationship between discharge energy and surface integrity evolution during WEDM of nickel-based superalloys. Increasing discharge energy intensifies melt pool formation and resolidification dynamics, leading to thicker recast layers, enhanced elemental redistribution, elevated tensile residual stresses, and greater hardness deviations. These coupled effects ultimately increase crack susceptibility in the thermally affected surface layer.

The following sections critically analyze recast layer characteristics, microhardness evolution, residual stress development, elemental redistribution, and surface chemistry modifications across various nickel-based superalloys, emphasizing discharge-energy-dependent mechanisms and material-specific responses.



Figure 2 Conceptual schematic illustrating the discharge-energy-driven evolution of surface integrity in WEDM of nickel-based superalloys.

5. Recast Layer Thickness

Recast layer formation is an inherent metallurgical consequence of Wire Electrical Discharge Machining (WEDM), resulting from rapid melting and subsequent resolidification of surface material under intense thermo-electrical discharges. The resulting white layer is microstructurally distinct from the bulk substrate and is typically characterized by brittleness, tensile residual stresses, entrapped debris, and micro-crack networks. These features collectively degrade fatigue resistance, corrosion performance, and long-term structural reliability—particularly critical in aerospace and turbine applications.

To illustrate this thermal erosion mechanism, **Figure 3** depicts the WEDM process, subsurface zonal distribution, and recast layer formation sequence. Spark discharges within the dielectric gap generate localized plasma channels that melt the superalloy matrix **Figure 3(A)**. Although dielectric flushing expels most molten material, residual liquid rapidly quenches on the surface, forming the porous, micro-cracked Recast Layer (White Layer) ($t_R \approx$ a few to tens of μm) **Figure 3(B)–(C)**. Beneath this layer, the Heat-Affected Zone (HAZ) undergoes steep thermal cycling and microstructural alterations without melting, while the deeper Unaffected Base Material retains its original parent microstructure.

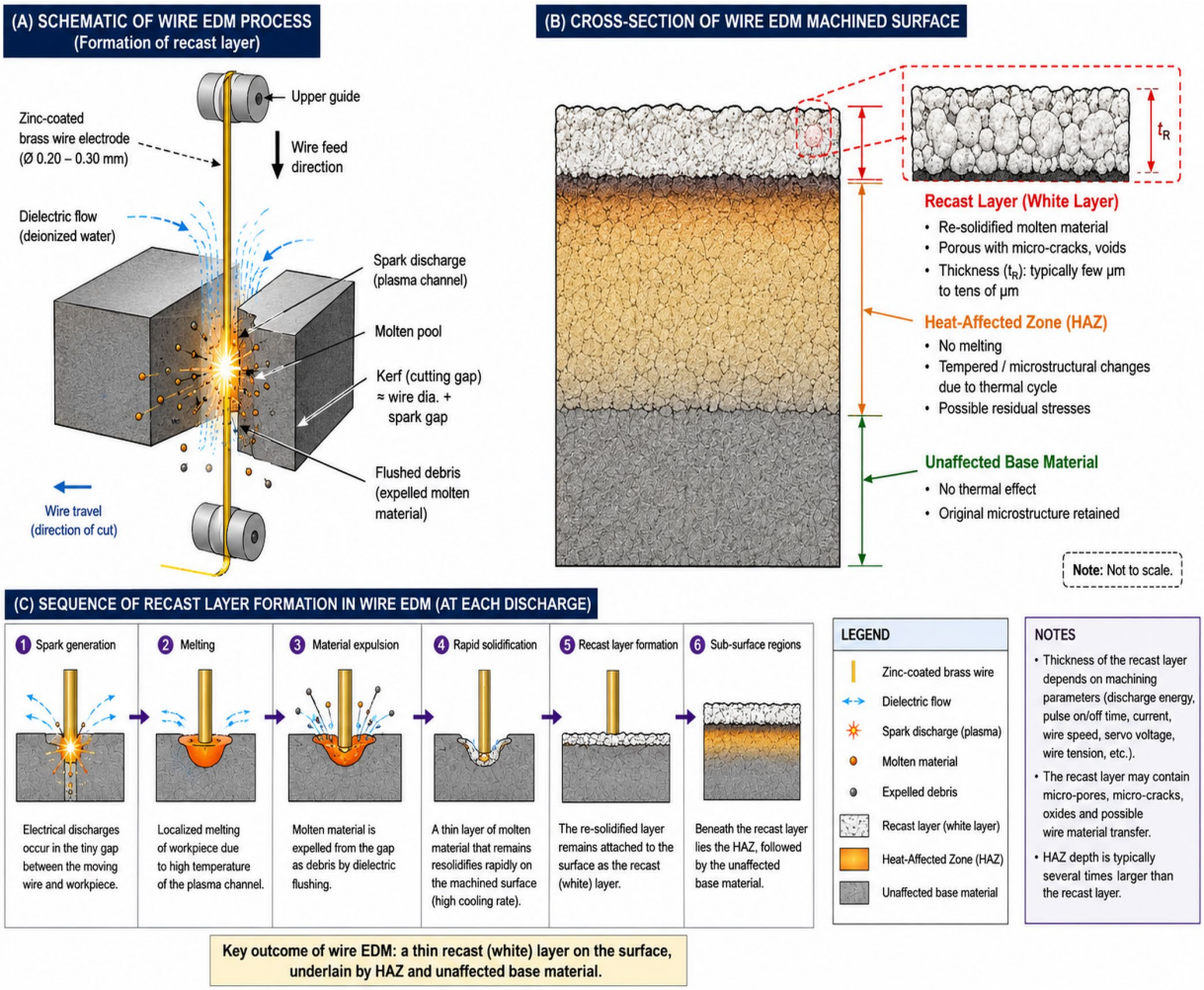


Figure 3 WEDM surface integrity evolution: (**A**) Process and kerf schematic, (**B**) Subsurface zonal breakdown (Recast Layer, HAZ, and Unaffected Base Material), and (**C**) Step-by-step single-discharge recast layer formation sequence.

5.1 Energy-Dependent Behavior

Across all investigated nickel-based superalloys, recast layer thickness (RLT) exhibits a strong and systematic dependence on discharge energy per spark, primarily governed by pulse-on time and peak current. Three distinct energy regimes can be identified:

- Low-energy / trim-cut / stable regimes (≈ 1–6 μm): Optimized parameters and multi-trim strategies significantly restrict thermal penetration depth. Alloys such as Inconel 939, Inconel 625, and Inconel 718 commonly exhibit RLT values between ~1.7 and 5.7 μm under stabilized conditions. Successive trim passes frequently reduce the white layer to 2–3 μm or render it nearly negligible. Enhanced flushing and extended pulse-off time improve molten material evacuation and suppress excessive resolidification.
- Moderate discharge energy (≈6–17 μm): Under controlled roughing conditions, RLT typically falls within this intermediate range. Inconel 718 frequently exhibits thicknesses of 5–9 μm (average ~7 μm), while Nimonic-90 and Nimonic C-263 show values around 10–12 μm. Although relatively uniform, such layers may still contain micro-voids and localized cracking.
- High-energy / aggressive roughing (≈ 20–50 μm): Elevated pulse-on time, increased peak current, and insufficient flushing markedly intensify thermal loading, producing thick, irregular, and porous recast layers. Inconel 706 and Inconel 690 demonstrate the highest sensitivity, with RLT reaching up to ~50 μm. B1914 and Nimonic C-263 similarly exhibit 20–40 μm under high spark energy. These layers are highly crack-prone and generally unsuitable for service without subsequent finishing or post-processing.

5.2 Alloy-Specific Sensitivity

While discharge energy remains the dominant governing parameter controlling recast layer formation during WEDM, the intrinsic thermophysical properties and strengthening mechanisms of the workpiece material significantly influence the extent, morphology, and integrity of the resolidified layer. Consequently, alloys subjected to identical machining conditions often exhibit different recast layer characteristics owing to differences in their thermal response and metallurgical behavior. Precipitation-strengthened nickel-based superalloys, such as Inconel 718 and Udimet 720, generally exhibit relatively moderate recast layer thicknesses under comparable discharge energies, whereas alloys including Inconel 706, Inconel 690, and B1914 frequently display greater variability and comparatively thicker recast layers due to differences in thermal transport and solidification behavior.

To summarize the material-dependent responses observed during WEDM, **Table 1** presents the principal thermophysical, thermodynamic, fluid-dynamic, and mechanical properties governing surface integrity together with their direct influence on recast layer evolution. Among these, thermal conductivity and thermal diffusivity are the most influential heat transport properties because they determine the rate of heat dissipation from the discharge zone. Lower values restrict conductive heat transfer, resulting in greater heat accumulation, larger molten pools, thicker recast layers, and wider heat-affected zones (HAZ). The melting temperature, melting range, latent heat of fusion, and specific heat capacity govern the energy required for melting and resolidification, thereby influencing the volume of molten material available for recast layer formation. In alloys exhibiting a broad solidification temperature range, prolonged solidification promotes micro segregation of low-melting constituents (e.g., Nb-rich Laves phases in certain nickel-based superalloys), thereby increasing the susceptibility to hot tearing and solidification cracking.

The viscosity and density of the molten metal further govern melt pool dynamics and material expulsion during dielectric flushing. Higher viscosity or density reduces the efficiency of molten material removal, allowing a larger fraction of the melt to resolidify on the machined surface and form a thicker recast layer. Furthermore, the coefficient of thermal expansion and elastic modulus control thermal strain and stress development during rapid dielectric quenching. Large thermal contraction combined with high material stiffness generates significant tensile residual stresses that promote microcrack initiation and propagation within the brittle recast (white) layer. In addition, metallurgical features such as carbide morphology and the stability of strengthening precipitates (γ' and γ'') influence high-temperature softening behavior, melt pool stability, and solidification kinetics, thereby affecting recast layer continuity, porosity, crack susceptibility, and defect density.

Overall, these observations demonstrate that alloy chemistry and material properties modify—but do not override—the fundamentally energy-driven mechanism of recast layer formation. Instead, the final recast layer thickness and morphology result from the combined effects of discharge energy and the inherent thermophysical and metallurgical characteristics of the workpiece material.

5.3 Role of Secondary Parameters

Secondary process variables further refine recast evolution. Increased pulse-off time and optimized servo voltage enhance cooling and debris evacuation, limiting excessive recast accumulation. Wire characteristics influence local heat distribution: coated wires often reduce RLT during roughing, whereas larger wire diameters may increase thickness due to higher localized thermal input. Machining stability is particularly critical; improved spark stability has been shown to reduce RLT by more than 80% in certain Inconel 718 studies.

5.4 Comparative Perspective and Synthesis

Figure 4 comparatively quantifies recast layer thickness across multiple nickel-based superalloys processed by WEDM, revealing a consistent discharge-energy-controlled hierarchy. Thin layers (≈ 1–6 μm) are achieved under stabilized low-energy regimes,

Table 1 Summary of governing thermophysical properties of nickel-based superalloys and their combined mechanisms on WEDM surface integrity.

Thermophysical Property	**Combined Mechanism & Surface Integrity Impact**
Thermal Conductivity & Thermal Diffusivity	Lower values trap conductive heat at the spark site, producing larger melt pools, thicker recast layers, steeper quenching thermal gradients, and deeper heat-affected zones.
Solidification Range	Broader range expands the two-phase mushy zone, driving interdendritic micro-segregation of low-melting phases (such as Laves phase) and heightening hot-tearing risk.
Latent Heat of Fusion & Melting Point	Higher values elevate the thermal energy required per unit mass melted, reducing melted volume, producing smaller craters, and lowering surface roughness.
Specific Heat Capacity	Lower values accelerate the temperature rise to the melting point, resulting in deeper discharge craters, higher melted volume fractions, and thicker recast layers.
Thermal Expansion & Elastic Modulus	Higher values amplify volumetric contraction during rapid quenching, generating severe tensile residual stresses and increasing vertical micro-crack density in the recast layer.
Molten Metal Viscosity & Fluidity	Higher viscosity resists liquid pool flushing, retaining a larger volume of un-ejected melt in craters to form thicker, non-uniform recast layers with higher surface roughness.
Material Density	Higher density increases the inertial resistance of the liquid pool during flushing, reducing ejection efficiency and leaving behind uneven recast layer morphology.
Electrical Resistivity	Higher values intensify localized resistive heating, accelerating local energy buildup, driving plasma channel expansion, and increasing spark energy density.

whereas aggressive conditions induce substantial thermal penetration (up to ~50 µm in Inconel 706 and Inconel 690). Alloys such as Inconel 625 and Inconel 939 exhibit narrower variability, suggesting more stable melt pool behavior and effective thermal dissipation. Precipitation-strengthened systems (e.g., Nimonic and Udimet alloys) show moderate sensitivity, while B1914 displays pronounced variability under equivalent energy input.

To synthesize these material-dependent variations, the min–max scatter in recast layer thickness across various nickel-based superalloys must be understood through the lens of local discharge thermodynamics, alloy melting points, and transient quenching kinetics. During spark erosion, high-energy plasma discharges generate localized surface temperatures (8,000 to 12,000 degrees Celsius) that far exceed the melting point of the target substrate, inducing instantaneous melting and severe thermal superheating. As demonstrated by Kumar et al. [56] during machining of Inconel 825, increasing the discharge energy elevates localized thermal flux well beyond the material melting threshold, expanding the volume of the transient molten pool and increasing both recast layer thickness (from 20.99 to 34.62 µm) and surface crack density (from 0.0016 to 0.0138 µm/ µm^2).

When plasma discharge terminates, the surrounding dielectric fluid subjects this superheated molten layer to ultra-fast quenching rates. For superalloys characterized by higher melting points combined with lower thermal conductivity (such as Inconel 706, Inconel 690, and B1914 in **Figure 4**), a significant fraction of the superheated liquid pool resists dielectric flushing due to rapid skin solidification, remaining trapped within the discharge crater. During this rapid solid-state transformation, steep thermal gradients and severe volumetric thermal contraction generate high tensile residual stresses that exceed the yield strength and plastic deformation limit of the material, initiating dense networks of vertical micro-cracks across the resolidified white layer. Conversely, superalloys exhibiting lower melting ranges or narrower solidification intervals allow for more complete dielectric flushing and reduced thermal stress retention, yielding characteristically thinner and tighter recast layer data ranges (such as Inconel 625 and Inconel 939). Ultimately, a detailed discussion of the relationship between melting point temperatures and material thermodynamic properties provides valuable physical insight into the observed variations in recast layer thickness.

The graphical trend reinforces that spark energy density governs recast evolution, with alloy thermophysical properties modulating—but not superseding—the primary energy dependence. Optimized multi-trim strategies effectively suppress recast severity across all systems.

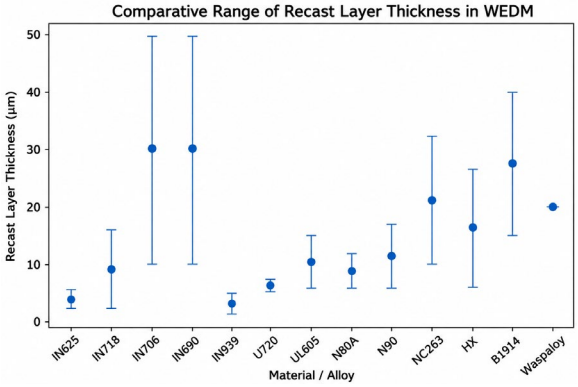


Figure 4 Comparative min–max range of recast layer thickness in WEDM of various nickel-based superalloys, highlighting the dominant influence of discharge energy and alloy-dependent variability.

Collectively, the evidence establishes a clear hierarchical influence governing recast layer formation:

Discharge Energy ≫ Flushing Efficiency > Wire Characteristics > Alloy Chemistry

Recast layer thickness across nickel-based superalloys spans approximately 1–50 µm depending on machining conditions. Achieving aerospace-grade surface integrity generally requires maintaining RLT below ~5–6 µm, attainable through controlled low-energy regimes combined with multi-trim finishing strategies.

Overall, recast layer thickness emerges as the most immediate and quantifiable indicator of WEDM-induced surface alteration. While discharge energy dictates the primary thermal input, alloy chemistry and machining stability determine the severity of metallurgical transformation and defect formation within the resolidified layer. Accordingly, controlling RLT is not merely a matter of process optimization but a prerequisite for ensuring structural reliability in critical high-temperature applications.

These findings highlight the necessity of integrating energy-aware parameter selection with alloy-specific considerations to minimize surface damage. The subsequent sections examine how recast layer evolution interacts with microhardness variation and elemental redistribution, providing a comprehensive framework for understanding WEDM-induced surface integrity mechanisms.

6. Microhardness Evolution

The reviewed literature demonstrates that microhardness variation in WEDM-processed nickel-based superalloys is strongly governed by discharge energy, machining stability, and alloy chemistry, although the direction and magnitude of change are not universally uniform. Traditionally, the white/recast layer is expected to exhibit higher hardness than the bulk material due to rapid solidification, microstructural refinement, and carbide or oxide formation. However, in precipitation-strengthened superalloys, surface and subsurface softening frequently dominate over hardening, particularly under high discharge energy.

In Inconel 718 and Inconel 706, multiple investigations report pronounced subsurface softening. For Inconel 706, hardness decreased from ~425 HV (bulk) to ~192 HV near the machined surface, with the softened region extending approximately 70–80 µm depending on discharge energy. Similarly, Inconel 718 exhibited reduced hardness under unstable machining conditions (minimum ~130 HV versus ~180 HV bulk), whereas stable machining largely preserved subsurface integrity. This softening is attributed to repeated thermal cycling, rapid quenching by the dielectric, elemental redistribution, tensile residual stresses, and limited secondary carbide strengthening due to relatively low carbon content.

Comparable softening behavior has been observed in Nimonic-90, Nimonic C-263, Inconel 690, Hastelloy X, and Udimet-L605, where increasing pulse-on time and peak current intensified thermal degradation and expanded the softened heat-affected zone (HAZ). In Nimonic C-263, surface hardness decreased to ~153 HV during rough cutting but recovered after post-processing, confirming that degradation is largely confined to the thermally altered superficial layer.

Conversely, localized hardening of the recast layer has been reported in Waspaloy and selected Inconel 625 conditions, where rapid solidification and oxide/carbide formation increased surface hardness. Nevertheless, such hardened layers remain brittle and susceptible to fatigue cracking. Advanced nanoindentation and micro-pillar compression testing on Inconel 718 further reveal that, despite apparent subsurface softening in conventional microhardness profiles, the resolidified recast layer itself can exhibit significantly enhanced compressive strength (up to ~2.2 times the bulk strength), highlighting pronounced microstructural heterogeneity within the superficial layer.

Subsurface microhardness profiling of Inconel 718 provides a representative example of this energy-dependent response (**Figure 5**). To evaluate subsurface metallurgical integrity, **Figure 5** illustrates depth-wise microhardness variations across three distinct machining stability regimes (designated as Lv_1, Lv_3, and Lv_5). As categorized by Abhilash and Chakradhar [26], Lv_1 represents the least stable machining state (pulse-on time of 116 µs, pulse-off time of 42 µs, servo voltage of 40 volts), Lv_3 denotes intermediate stability (110 µs pulse-on time, 46 µs pulse-off time, 50 volts servo voltage), and Lv_5 defines the most stable machining condition (104 µs pulse-on time, 50 µs pulse-off time, 60 volts servo voltage).

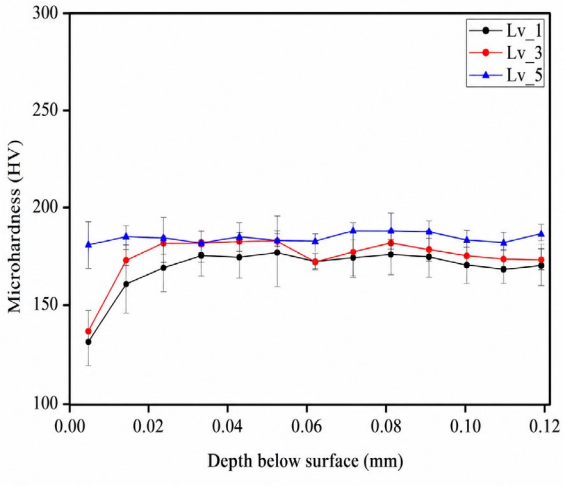


Figure 5 Subsurface microhardness profiles of machined specimens across various machining stability levels: Lv_1 (Level 1, least stable), Lv_3 (Level 3, intermediate stability), and Lv_5 (Level 5, most stable) [26]. Reprinted from [26] under the Creative Commons CC BY-NC-ND 4.0 license.

Under unstable machining conditions (Lv_1 and Lv_3), high localized spark energy fluctuations and sluggish debris evacuation exert a higher thermal impact on the immediate subsurface. High heat accumulation induces over-tempering and resolutioning of strengthening precipitates within the heat-affected zone, causing hardness to drop to a minimum of approximately 130 to 140 HV at the immediate surface before recovering to base levels within 35 to 40 micrometers (0.035 to 0.040 mm). Beyond a depth of 40 µm, thermal dissipation attenuates completely, and microhardness stabilizes across the unaltered parent material at approximately 180 HV. In contrast, the most stable machining regime (Lv_5) suppresses localized thermal accumulation and preserves subsurface microstructure, producing a nearly uniform hardness profile (maintaining approximately 185 to 190 HV directly from the immediate surface into the bulk depth) with negligible alteration [26].

Although **Figure 5** pertains specifically to Inconel 718, it exemplifies the broader trend observed across nickel-based superalloys—namely, that machining stability and discharge energy critically determine the depth and severity of subsurface mechanical degradation [26].

Overall, microhardness evolution in WEDM of nickel-based superalloys can be broadly classified into three distinct response behaviors. In certain alloys such as Inconel 706, Inconel 690, and Nimonic series, surface softening tends to dominate under high discharge energy conditions due to excessive thermal exposure, phase instability, and possible dissolution of strengthening precipitates. In contrast, alloys like Inconel 718 and additively manufactured Udimet 720 exhibit minimal deviation in microhardness when processed under optimized machining conditions, reflecting a balanced thermal input and stable microstructural response. Meanwhile, materials such as Waspaloy and selected cases of Inconel 625 demonstrate localized recast-layer hardening accompanied by increased brittleness, primarily attributed to rapid solidification, elemental redistribution, and the formation of hard but crack-prone phases within the recast layer.

Thus, microhardness behavior is not governed solely by the presence of a recast layer but by the complex interplay between discharge energy, precipitation-strengthening mechanisms, elemental redistribution, thermal conductivity, and machining stability. Excessive discharge energy promotes deeper softening and mechanical degradation, whereas controlled low-energy regimes mitigate thermal damage and preserve subsurface structural integrity.

The heatmap compares microhardness distribution across multiple nickel-based superalloys following WEDM (**Figure 6**). Alloys such as Inconel 625, Udimet 720, and Waspaloy demonstrate localized recast-layer hardening due to rapid solidification and carbide/oxide formation, whereas Inconel 706, Inconel 718, and Nimonic alloys exhibit subsurface softening associated with thermal degradation and residual stress development.

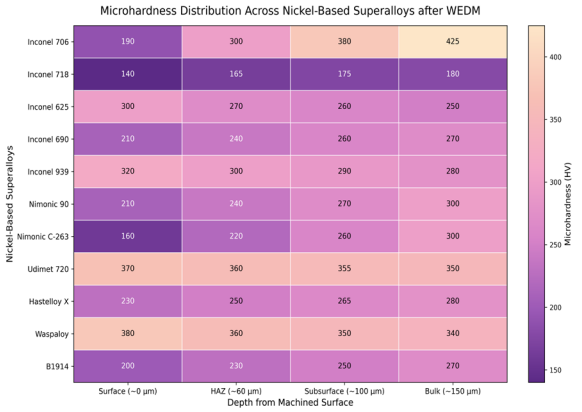


Figure 6 Heatmap illustrating microhardness variation with depth in representative nickel-based superalloys after WEDM, highlighting alloys exhibiting surface hardening, softening, or stable hardness behavior.

7. Elemental Redistribution

Elemental redistribution during WEDM is governed by electrode wear, dielectric decomposition, and intense thermo-electrical interactions within the plasma channel. The repeated melting and rapid resolidification inherent to spark erosion promote transfer of electrode-derived elements—primarily Cu and Zn from brass or zinc-coated wires—along with oxygen and carbon species generated from dielectric breakdown. Owing to extremely high cooling rates, these compositional modifications are largely confined to the recast layer; however, they substantially influence surface chemistry, residual stress development, and near-surface mechanical behavior.

In precipitation-hardened alloys such as Inconel 718 and Inconel 706, high discharge energy induces pronounced Cu–Zn enrichment and oxygen incorporation within the recast layer, accompanied by localized depletion of base alloying elements (Ni, Cr, Fe). The magnitude of redistribution decreases significantly under trim-cut strategies and improved machining stability, confirming strong discharge-energy dependence. Similar electrode-to-workpiece material transfer has been observed in Inconel 690 and Inconel 617, where detectable Zn and Cu concentrations appear despite negligible bulk presence, correlating with increased recast layer thickness and surface softening.

Alloy chemistry strongly modulates redistribution behavior. Nimonic 80A and Nimonic C-263 exhibit substantial elemental diffusion under aggressive machining, whereas Nimonic 90 demonstrates comparatively stable surface chemistry, suggesting enhanced resistance to compositional alteration. In boron-containing alloys such as B1914, complex redistribution involving Al, B, Ti, Cr, and Mo has been

reported, highlighting the influence of alloying elements on resolidification kinetics and local phase evolution.

Selective oxidation further contributes to chemical modification of the recast layer. Oxides such as Cr_2O_3, TiO_2, Nb_2O_5, and MoO_3 are frequently detected in Inconel 625 and 718, indicating strong plasma–dielectric interaction and localized high-temperature oxidation. These oxide phases alter surface hardness, embrittlement tendency, and corrosion resistance.

A representative example is provided by NiTi shape memory alloy, where Energy Dispersive X-ray Spectroscopy (EDS) spot analysis quantifies foreign element atomic content (FEAC = Cu + Zn + C + O) within the recast layer [48]. Elemental composition measured across representative surface locations indicates that localized composition varies subtly depending on crater morphology; regions situated over re-solidified debris clusters capture higher concentrations of wire-derived brass transfer (Cu, Zn) and dielectric breakdown products (C, O), whereas smoother, flushed matrix regions display higher retention of the parent substrate matrix (Ni, Ti) [48].

As discussed in [48], the incorporation of Cu and Zn from the brass wire electrode, together with C and O from dielectric decomposition, increases markedly with higher pulse-on time. At an elevated pulse-on time of 1.35 μs, high thermal energy input accelerates brass wire erosion and hydrocarbon dielectric cracking, producing an aggressive average FEAC of 41.05% (weight percentages of 9.98% Cu, 1.35% Zn, 12.47% O, and 17.65% C) [48]. Conversely, lowering the pulse-on time to 0.35 μs limits spark-induced tool wear and dielectric breakdown, cutting the average FEAC by nearly half to 21.15% while maintaining superior base alloy retention (47.59% Ni and 31.26% Ti) [48]. Furthermore, higher pulse-off time and spark gap voltage (SV) reduce contamination by enhancing cooling and flushing efficiency, while wire feed rate and wire tension exert minimal influence [48].

Although these specific compositional trends are detailed in [48] for the NiTi system, they exemplify the broader mechanism of energy-driven compositional modification common to nickel-based superalloys.

Collectively, these findings demonstrate that elemental redistribution is strongly discharge-energy dependent and highly alloy-specific. Electrode material transfer, oxygen enrichment, and selective oxidation jointly dictate recast layer chemistry, which in turn governs microhardness evolution, crack susceptibility, and long-term surface reliability. Therefore, effective control of discharge energy and post-processing strategies is essential to mitigate chemical degradation and ensure functional integrity of WEDM-processed superalloys.

8. Residual Stresses

Residual stresses generated during WEDM of nickel-based superalloys arise from rapid localized melting and extremely high cooling rates within the plasma–dielectric environment. The steep thermal gradients between the resolidified recast layer and the cooler substrate produce a depth-dependent residual stress field, typically characterized by high tensile stresses at the immediate surface transitioning toward lower tensile or partially compressive stresses within the underlying heat-affected zone (HAZ).

Reported measurements (primarily via XRD and hole-drilling methods) indicate that surface tensile residual stresses in WEDM-processed nickel-based superalloys generally range from approximately +200 to +800 MPa, depending on discharge energy and alloy system. Under aggressive rough-cut or unstable machining conditions, peak tensile stresses approaching +600–900 MPa have been reported in alloys such as Inconel 718 and Inconel 706, particularly when associated with thick (>20 μm) recast layers. In contrast, optimized low-energy or multi-trim strategies typically reduce surface tensile stresses to the range of +100 to +300 MPa, with rapid stress decay within the first 20–50 μm below the surface.

In precipitation-strengthened alloys such as Inconel 718, tensile residual stresses are predominantly confined to the recast layer and a thin HAZ under controlled conditions, whereas high-energy regimes promote deeper thermal penetration and elevated tensile stress accumulation linked to crack initiation. Similar behavior has been observed in Inconel 706, where thicker resolidified layers correspond to higher stress magnitudes and increased crack susceptibility.

Alloys such as Inconel 625 and Hastelloy X, which exhibit comparatively higher thermal conductivity and solid-solution strengthening, often show reduced stress localization under equivalent energy input, with reported tensile stresses generally remaining toward the lower end of the above range. Conversely, Nimonic C-263 and B1914, which form thicker recast layers under high spark energy, exhibit higher tensile stress concentration and pronounced micro-crack networks.

Figure 7 illustrates the typical distribution of residual stresses with depth in WEDM-processed nickel-based superalloys. The surface recast layer generally exhibits tensile residual stresses due to rapid melting and constrained solidification during spark discharge. Moving into the heat-affected zone (HAZ), the stress magnitude decreases and often transitions toward compressive residual stresses as thermal gradients relax. Finally, in the base material, the residual stress gradually approaches equilibrium ($\sigma \approx 0$). The comparative curves indicate that alloys such as Inconel 706 and Inconel 718 tend to develop higher surface tensile stresses, while alloys with higher thermal conductivity such as Inconel 625 and Hastelloy X show comparatively lower stress concentration and faster stress relaxation with depth.

Across all systems, increasing pulse-on time and peak current consistently intensify tensile residual stress magnitude, while low-energy multi-trim

strategies reduce stress concentration by limiting melt depth and enhancing flushing stability. Beneath the tensile surface layer, partial compressive or near-zero stress states are sometimes observed due to thermal contraction gradients and plastic accommodation.

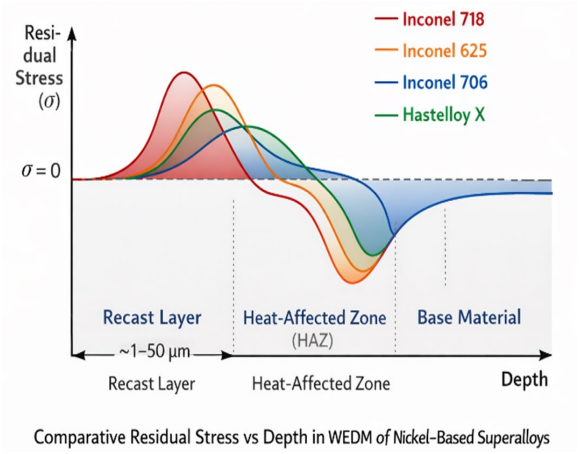


Figure 7 Comparative schematic of residual stress distribution with depth in WEDM-processed nickel-based superalloys, showing tensile stresses in the recast layer, stress transition within the HAZ, and gradual relaxation toward the base material.

Residual stress severity is therefore primarily discharge-energy driven, with alloy thermophysical properties and strengthening mechanisms modulating stress magnitude, depth penetration, and crack susceptibility. Residual stresses represent a critical intermediate link in the energy–microstructure–mechanical performance framework governing WEDM-induced surface integrity in nickel-based superalloys.

9. Critical Analysis of Contradictions, Discrepancies, and Measurement Reliability in Surface Integrity

A critical synthesis of published WEDM literature on nickel-based superalloys reveals substantial scatter and apparent contradictions in reported surface integrity outcomes. Rather than indicating simple experimental error, these variations stem from complex thermal-mechanical energy interactions, dielectric fluid hydrodynamics, alloy-specific thermophysical properties, and measurement technique limitations.

9.1 Recast Layer Thickness (RLT) Discrepancies and Measurement Reliability

Reported RLT values vary widely from approximately 1 µm to >50 μm. Discharge energy acts as the dominant governing parameter; aggressive rough-cutting modes generate deep melt pools and thick recast layers, whereas controlled low-energy and multi-trim strategies suppress RLT below 5–6 µm to meet aerospace-grade requirements. Furthermore, dielectric hydrodynamics (flushing pressure and thermal quenching rates) and spark instability (localized arcing) dictate whether molten metal is effectively flushed or re-solidified onto the cut surface.

The choice of measurement technique introduces substantial technical uncertainty into published RLT values. Optical microscopy provides rapid screening but suffers from insufficient spatial resolution (>1 μm) and optical halation at specimen edges, rendering it unreliable for thin recast layers (<5 μm). Standard cross-sectional SEM [14] using linear single-peak measurements introduces high subjective bias, as taking values at isolated re-solidified peaks severely overestimates mean RLT. Furthermore, standard mechanical polishing (ASTM E3) frequently induces specimen preparation artifacts, such as edge rounding or ductile material smearing across the recast boundary. To achieve high measurement reliability, evaluating cross-sectional SEM images [14] using area-based averaging in ImageJ ($RLT = RLA/RLL$, total recast area divided by evaluation length) provides a statistically representative value that mitigates localized crater skewing. For maximum precision, Focused Ion Beam (FIB-SEM) micro-machining completely eliminates mechanical polishing artifacts and edge rounding, exposing pristine cross-sectional interfaces for exact RLT quantification.

9.2 Microhardness Alterations: Softening vs. Hardening Contradictions and Testing Reliability

Literature presents opposing trends regarding subsurface microhardness evolution. Microhardness response is not universally hardening-dominated; subsurface thermal softening is common under high-energy conditions, where localized thermal dumping induces precipitate resolutioning and heat-affected zone (HAZ) annealing (causing hardness to drop to ~130–140 HV). Conversely, localized recast layer hardening occurs due to rapid dielectric quenching and wire electrode element transfer, which increases localized surface brittleness.

Evaluating microhardness near the immediate subsurface carries significant experimental uncertainty depending on test parameters. Standard Vickers microhardness testing utilizing indentation loads greater than 100 g produces large indentations that often exceed the thickness of the recast layer, capturing a combined response of the recast layer, HAZ, and underlying bulk substrate [13]. Additionally, testing extremely close to the specimen edge under high loads introduces indentation size effects (ISE) and edge deflection errors. To ensure high measurement reliability, low-load micro-indentation (10–25 g) or continuous depth-sensing nanoindentation must be employed. Nanoindentation allows sub-micron spatial resolution, enabling accurate mapping of steep hardness gradients across ultra-thin recast zones (<20 μm) without substrate interference [13].

9.3 Elemental Redistribution Discrepancies and Characterization Fidelity

Foreign element atomic content (FEAC = Cu + Zn + C + O) exhibits significant scatter across studies (10–45%) Elemental transfer is strongly discharge-energy dependent and largely confined to the recast layer, directly influencing hardness variations and crack susceptibility. Alloy chemistry modulates the severity of contamination—for instance, precipitation-strengthened alloys (e.g., Inconel 718, Udimet 720) maintain higher structural stability than alloys like Inconel 706 or B1914 under aggressive regimes—though energy settings remain the primary driver.

Discrepancies in reported FEAC values frequently stem from compositional sampling methods. Single-spot Energy Dispersive X-ray Spectroscopy (EDS) measurements taken over localized, un-ejected debris pockets over-report wire transfer (Cu, Zn) and dielectric breakdown products (C, O), whereas spot measurements over smooth, well-flushed matrix regions under-report contamination. High characterization reliability is achieved by replacing single-spot analysis with multi-point area EDS averaging or depth-wise EDS line scans across cross-sections [14]. For chemical state resolution at the outermost atomic layers (<10 nm), X-ray Photoelectron Spectroscopy (XPS) and Transmission Electron Microscopy equipped with EDS (TEM-EDS) provide definitive separation between surface oxide/carbide films and the underlying parent matrix [15],[16].

9.4 Residual Stress States and Profiling Accuracy

Surface tensile residual stresses are predominantly concentrated within the recast layer and scale directly with discharge energy and recast thickness, frequently reaching several hundred MPa under aggressive regimes. Residual stress distribution is highly depth-dependent, exhibiting rapid decay toward the unaltered bulk material. Mismatch in alloy thermophysical properties (thermal conductivity, coefficient of thermal expansion) critically influences stress localization, thermal contraction, and relaxation behavior.

Measuring residual stress profiles in WEDM surfaces involves major technical challenges. Standard laboratory X-ray Diffraction (XRD) using the $\sin^2\psi$ technique relies on X-ray penetration depths that typically exceed 5–10 μm [10],[11], effectively averaging the stress state of the recast layer with the underlying heat-affected zone. Furthermore, mechanical sectioning of specimens for cross-sectional analysis causes localized strain relaxation, altering the true residual stress field [10]. High profiling reliability requires incremental ring-core or micro-hole drilling combined with electronic speckle pattern interferometry (ESPI) to capture true depth-wise stress gradients. Alternatively, high-energy Synchrotron XRD enables sub-micron spatial resolution and non-destructive depth profiling, accurately resolving steep tensile-to-compressive stress transitions directly beneath the recast layer [12].

10. Synthesis of Recast Layer Thickness, Microhardness, Elemental Redistribution, and Residual Stress

The integrated evaluation of recast layer thickness (RLT), microhardness evolution, elemental redistribution, and residual stress reveals a strongly coupled process–structure–property relationship in WEDM of nickel-based superalloys. Increasing discharge energy intensifies thermal input, resulting in thicker recast layers, enhanced Cu–Zn transfer, and increased oxygen incorporation. These modifications alter resolidification behavior, generate high surface tensile residual stresses due to constrained shrinkage, and influence near-surface phase stability, thereby governing subsurface mechanical response. Although thicker recast layers generally correspond to greater hardness deviation and higher tensile stress, the severity of degradation remains alloy-dependent, controlled by precipitation strengthening mechanisms, alloy chemistry, and thermophysical properties. Crucially, the mechanistic pathways governing these variations differ fundamentally between niobium-rich, γ''-precipitate-strengthened grades (e.g., Inconel 718 and Inconel 706) and solid-solution or γ'-strengthened alloys (e.g., Inconel 625 and Inconel 690). In Inconel 718 and 706, the intense thermal pulses induce metastable dissolution and over-aging of the body-centered tetragonal γ'' (Ni_3Nb) strengthening phases within the heat-affected zone (HAZ), leading to localized micro-softening and steep thermal expansion mismatches that amplify peak tensile residual stress levels. Conversely, solid-solution-strengthened Inconel 625 and high-chromium Inconel 690 possess distinct thermophysical profiles—characterized by lower thermal conductivities, altered melting ranges, and higher chromium contents—which alter plasma spark energy dissipation, decrease molten pool stability, and modify dielectric quenching kinetics. These thermophysical characteristics result in altered recast layer consolidation, modified elemental segregation profiles (specifically Cr and Mo depletion), and reduced susceptibility to post-discharge thermal stress accumulation. Thus, discharge energy acts as the primary driver, while alloy characteristics modulate the resulting mechanical and structural response.

Figure 8 illustrates this coupled behavior through representative top-surface, cross-sectional SEM micrographs and energy-dispersive X-ray spectroscopy (EDX) spectra of WEDM-processed Inconel 718 [34]. The top-surface morphology (**Figure 8(a)**) exhibits re-solidified debris, gas pockmarks, and discharge craters, while the cross-sectional view (**Figure 8(b)**) clearly demarcates the recast layer boundary resting above the bulk material. EDX spectral analysis on the EDMed surface (**Figure 8(c)**) confirms substantial Cu (~10.5 wt%) and Zn (~5.8 wt%) enrichment originating from wire electrode erosion, along with pronounced oxygen incorporation (~12.1 wt%), signaling dielectric decomposition and localized oxidation.

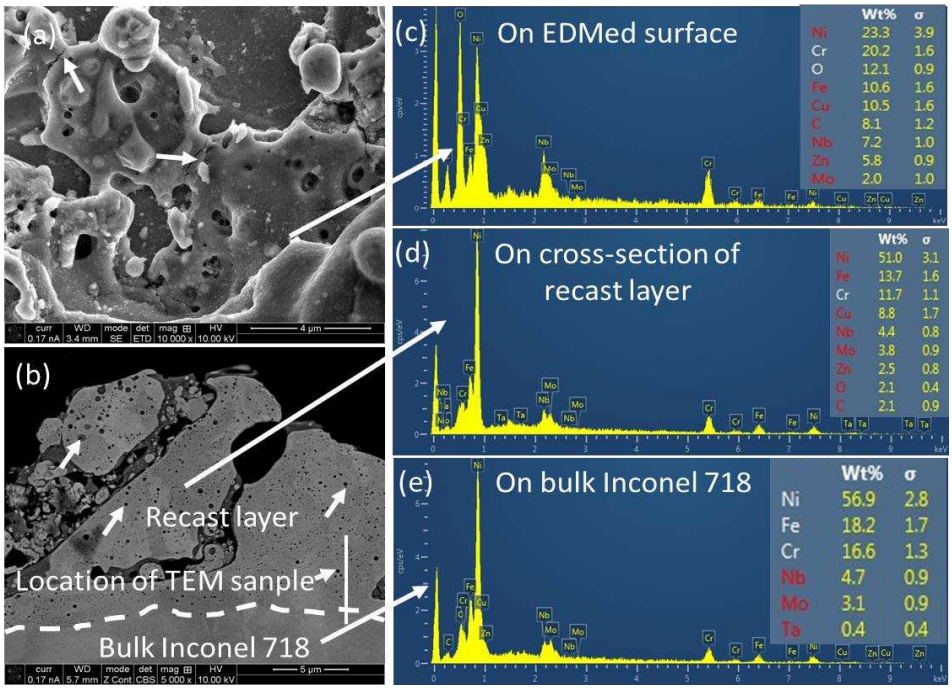


Figure 8 Representative features on the machined surface of Inconel 718 after WEDM on (**a**) cylindrical surface and (**b**) cross-section, together with energy-dispersive X-ray spectroscopy (EDX) spectra on (**c**) cylindrical surface, (**d**) cross-section, and (**e**) bulk material [34]. Reprinted from [34] under the Creative Commons CC BY license.

While cross-sectional EDX within the recast layer (**Figure 8(d)**) displays moderate retention of these migrated elements (Cu: ~8.8 wt%, Zn: ~2.5 wt%), comparison with the pristine bulk Inconel 718 baseline (**Figure 8(e)**) demonstrates clear composition-driven phase destabilization. This microstructural and chemical heterogeneity directly contributes to localized tensile residual stress concentrations. Although specific to Inconel 718, these observations typify the discharge-driven compositional and structural modifications observed across nickel-based superalloys.

Figure 9 synthesizes these multi-variable interaction dynamics using a six-metric radar plot comparing recast layer thickness (RLT) severity, microhardness alteration, residual stress intensity, crack density, elemental redistribution, and heat-affected zone (HAZ) depth across representative superalloys (IN718, IN706, IN690, NC263, and U720). Inconel 706 exhibits the most severe overall degradation profile (rated 5 across all metrics), characterized by thick recast layers, pronounced subsurface thermal softening, elevated tensile residual stress concentrations, and extended HAZ depths. Conversely, Inconel 718, Inconel 625, and Udimet 720 maintain tight, highly stable damage boundaries (ratings 1–2) under optimized pulse conditions. Inconel 690, Nimonic C-263, and B1914 demonstrate intermediate responses (ratings 3–4), where solid-solution strengthening and superior oxidation resistance mitigate severe crack network propagation despite moderate compositional transfer.

Complementing these observations, **Tables 2–3** provide a consolidated quantitative–qualitative breakdown across process parameters, confirming that higher discharge energy universally drives thicker recast layers, increased wire tool transfer, and elevated tensile residual stresses. Ultimately, these findings reveal that while discharge energy governs the absolute magnitude of surface damage, alloy chemistry and precipitation state dictate its volumetric extent—reinforcing a unified process–structure–property–stress framework essential for alloy-specific energy optimization in mission-critical aerospace and power generation applications.

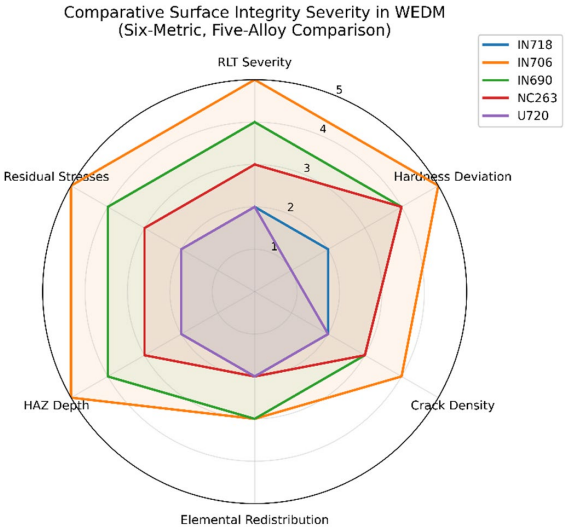


Figure 9 Radar chart illustrating comparative surface integrity severity (RLT, hardness deviation, residual stress, crack density, elemental redistribution, and HAZ depth) in WEDM-processed nickel-based superalloys.

Table 2 Integrated quantitative and qualitative comparison of recast layer thickness and microhardness behavior in WEDM-processed nickel-based superalloys.

Alloy (Reference)	**Recast Layer Thickness (µm)**	**Microhardness (HV)**
Inconel 706 [22],[23],[35],[36]	~10–50 (thick, non-uniform, highly energy-sensitive)	~425 → ~192 (severe subsurface softening; deep HAZ)
Inconel 718 [2],[21]	~2.6–15.9 (moderate; stability-dependent)	~180 → ~130 (unstable); ~180 (stable) (softening mitigated under stable conditions)
Inconel 625 [54]	~2.7–5.7 (thin, uniform)	~250 → ~280–320 (localized recast-layer hardening)
Inconel 690 [41]	~10–50 (thick, variable)	~221 → 122–171 (surface softening)
Inconel 939 [44]	~1.67–5.34 (thin, continuous)	Near bulk (minimal deviation)
Udimet 720 [20],[45]	~5.5–7.6 (moderate; reduced after trim)	~350–380 → ~360 (slight hardening/ stable)
Udimet-L605 [38]	~6–15 (moderate)	Surface softening (moderate degradation)
Nimonic 80A [27],[28]	~6 → ~12 (significant increase at high energy)	Surface softening (energy-dependent)
Nimonic 90 [29]	~6–17 (moderate to thick)	Significant softening at high energy
Nimonic C-263 [39],[40]	~10–32 (thick, crack-prone)	~293–314 → ~153 (severe softening)
Hastelloy X [42]	~6.4–26.4 (moderate to thick)	~212 → ~167 (surface softening; recovery with depth)
Inconel 617 [33]	Not quantified (morphology-dependent)	Surface softening with subsurface hardening
Waspaloy [43]	~20 (thick)	Recast-layer hardening (brittle behavior)
B1914 [37]	~15–40 (thick, irregular)	Surface softening
NiTi SMA [48]	Variable (process-dependent)	Softening/hardening depending on energy
AM Superalloys [44],[45]	Variable (anisotropy-dependent)	Modified hardness distribution

Table 3 Integrated quantitative and qualitative comparison of residual stress magnitude, and elemental redistribution in WEDM-processed nickel-based superalloys.

Alloy (Reference)	**Residual Stress (MPa)**	**Elemental Redistribution**
Inconel 706 [22],[23],[35],[36]	~500–800 (high tensile; deep penetration)	Strong Cu–Zn transfer; significant O enrichment
Inconel 718 [2],[21]	~200–500 (moderate tensile; reduced with stable machining)	Localized Cu–Zn enrichment; oxygen incorporation
Inconel 625 [54]	~100–300 (low tensile; shallow distribution)	Mild oxidation; limited elemental transfer
Inconel 690 [41]	~300–600 (moderate–high tensile; depth-dependent)	Cu–Zn contamination; oxide formation
Inconel 939 [44]	~200–400 (moderate tensile; shallow)	Limited redistribution under optimized conditions
Udimet 720 [20],[45]	~150–300 (low tensile; reduced by coated wire)	Reduced contamination with coated electrodes
Udimet-L605 [38]	~300–500 (moderate tensile)	Noticeable elemental diffusion
Nimonic 80A [27],[28]	~300–600 (moderate–high tensile)	Significant Cu–Zn transfer
Nimonic 90 [29]	~300–600 (moderate–high tensile)	Limited but energy-dependent redistribution
Nimonic C-263 [39],[40]	~400–700 (high tensile; crack susceptibility)	Strong oxidation and diffusion
Hastelloy X [42]	~200–400 (moderate tensile; decreases with depth)	Moderate redistribution
Inconel 617 [33]	~300–600 (tensile with localized compressive zones)	Strong elemental diffusion
Waspaloy [43]	~300–600 (moderate–high tensile)	Carbide/oxide enrichment
B1914 [37]	~500–800 (high tensile; deep penetration)	Significant elemental redistribution
NiTi SMA [48]	~200–600 (variable stress state)	Strong Cu–Zn, C, O incorporation
AM Superalloys [44],[45]	~200–600 (heterogeneous stress field)	Microstructure-dependent redistribution

11. Research Gaps, and Strategic Future Directions

Although significant progress has been made in understanding the surface integrity of nickel-based superalloys machined via WEDM, existing literature relies heavily on post-mortem experimental characterization and empirical optimization. To transition from trial-and-error processing to predictive, zero-defect manufacturing, future research must address critical knowledge gaps through advanced digital frameworks, real-time diagnostics, and physics-driven modeling.

11.1 Machine-Learning-Assisted Multi-Objective Optimization

Current parameter optimization studies predominantly utilize static statistical methods (e.g., Taguchi, Response Surface Methodology) that fail to capture complex non-linear interactions across variable discharge regimes. Future work must focus on integrating artificial neural networks (ANN) and deep machine learning architectures to model spark erosion kinetics in superalloys like Inconel 718 and Incoloy 800H [57–59]. Transitioning from empirical RSM models to physics-informed neural networks (PINNs) enables robust multi-objective optimization of pulse parameters (T_{on}, T_{off}) and servo voltage (SV), suppressing recast layer formation while maximizing cutting efficiency [52].

11.2 Digital Twins for Surface Integrity and Stress Profiling

Predictive modeling of subsurface damage remains constrained by computationally intensive thermo-mechanical finite element simulations. Developing real-time digital twins presents a vital frontier for non-destructive surface integrity prediction. By logging and analyzing process data during cutting, predictive frameworks can map geometrical accuracy and thermal penetration [60]. Furthermore, integrating physics-informed hybrid digital twins with multi-sensor intelligence enables adaptive, real-time control of energy deposition, allowing instantaneous estimation of subsurface thermal stress fields and recast layer evolution during process execution [61].

11.3 In-Situ Monitoring of Recast Layer Buildup and Discharge Dynamics

Existing studies evaluate surface defects post-machining, making real-time defect suppression impossible. High-frequency multi-sensor monitoring offers transformative potential for detecting instability before thermal damage occurs. Utilizing multi-sensor condition monitoring systems enables real-time pulse classification and early detection of process failures [62]. Furthermore, tracking acoustic emission (AE) parameters during the spark erosion of heat-resistant alloys provides direct, non-invasive indicators of surface quality, allowing real-time identification of localized arcing and abnormal discharge concentrations that cause severe recast layer spikes (>40 μm)[63].

11.4 Alloy-Specific Metallurgical Energy Management

While existing literature (reviewed in Section 2.4) empirically documents how individual nickel superalloys—such as Inconel 706, B1914, and Udimet-L605—exhibit distinct recast morphology and crack susceptibility, current commercial WEDM systems still apply generic, static pulse settings across different material grades. To overcome the cross-alloy optimization limitations identified in prior studies, future research must shift from offline trial-and-error parameter tuning to closed-loop, alloy-specific energy management systems. Future hardware developments should target adaptive pulse generators equipped with real-time feedback controllers that dynamically adjust spark duration, peak current, and dielectric flushing rates based on the specific thermophysical properties (melting enthalpy, thermal conductivity, precipitate dissolution kinetics) of the target alloy [64],[65]. This next-generation approach will prevent localized thermal dumping, suppress wire-element migration (Cu–Zn diffusion), and minimize subsurface damage in heat-sensitive superalloys.

11.5 Hybrid WEDM Configurations for Enhanced Flushing and Recast Control

To surpass the fundamental thermal limitations of conventional WEDM, future research across the machining community must explore advanced hybrid processes. Integrating combined ultrasonic vibration and magnetic field assistance with low-speed WEDM (US-MF-LS-WEDM) presents substantial promise for accelerating debris clearance, stabilizing discharge gaps, and mitigating localized arcing [66]. Investigating these complex field couplings is essential to establish how simultaneous mechanical vibration and Lorentz force dynamics alter bubble collapse, minimize localized thermal dumping, and suppress both recast layer thickness (R_L) and micro-crack formation during the high-precision machining of complex superalloy geometries [66].

12. Findings from Present Research Study

A comprehensive synthesis of the literature on the WEDM of nickel-based superalloys reveals several critical insights and persistent gaps in the current state of knowledge:

- Underrepresented Superalloy Systems: Research on newly developed nickel-based superalloys—including advanced Haynes grades and single-crystal systems such as René N5—remains remarkably limited despite their growing deployment in high-temperature turbine and aerospace propulsion applications.
- Additively Manufactured (AM) Superalloys: Investigations into the WEDM post-processing of additively manufactured nickel-based superalloys are comparatively scarce, leaving a major gap in understanding how printed microstructures and anisotropic thermal responses react to spark erosion.

- Long-Term Performance Correlations: Functional, long-term performance relationships—specifically linking recast layer metallurgy, surface defects, and micro-cracking to mechanical fatigue life, creep resistance, and high-temperature oxidation behavior—remain insufficiently explored.
- Electrode-Derived Elemental Contamination: Quantitative control strategies for suppressing tool-side elemental transfer are not systematically established. High-temperature discharge plasma drives brass component migration (Cu–Zn diffusion causing liquid metal embrittlement) and dielectric pick-up (O/C incorporation), degrading surface integrity.
- Cross-Alloy Energy Metrics: While discharge energy (T_{on} and I_p) is consistently identified as the primary governing parameter, parameter optimization relies heavily on empirical, single-alloy testing rather than normalized, physics-based energy ratios that scale across varying thermophysical properties.

13. Conclusions

This review establishes a unified surface integrity framework for WEDM of nickel-based superalloys by integrating recast layer thickness (RLT), microhardness evolution, elemental redistribution, and residual stress development. The key conclusions are:

- Discharge energy is the dominant governing parameter, directly controlling RLT, elemental transfer, residual stress magnitude, and subsurface mechanical alteration.
- RLT varies widely (~1–50 μm) depending on machining regime; controlled low-energy and multi-trim strategies can reduce RLT below ~5–6 μm for aerospace-grade requirements.
- Surface tensile residual stresses are predominantly concentrated within the recast layer and scale with discharge energy and recast thickness, often reaching several hundred MPa under aggressive regimes.
- Residual stress distribution is depth-dependent, with rapid decay toward the bulk; alloy thermophysical properties influence stress localization and relaxation behavior.
- Alloy chemistry modulates severity but does not override energy dependence; precipitation-strengthened alloys (e.g., Inconel 718, Udimet 720) show greater stability than Inconel 706, Inconel 690, and B1914 under aggressive regimes.
- Microhardness response is not universally hardening-dominated; subsurface softening is common under high-energy conditions, while localized recast hardening may occur with increased brittleness.
- Elemental redistribution (Cu–Zn transfer and oxygen incorporation) is strongly discharge-energy dependent and largely confined to the recast layer, directly influencing hardness variation and crack susceptibility.
- Increasing discharge energy produces thicker recast layers, greater elemental transfer, higher tensile residual stress, and larger hardness deviations, ultimately increasing crack risk, with alloy properties modulating the severity of degradation.

Overall, achieving reliable surface integrity in WEDM of nickel-based superalloys requires transitioning from empirical tuning to mechanistic, alloy-specific energy management. Future research should integrate physics-based modeling with artificial intelligence, machine learning, and data-driven optimization frameworks to enable predictive and real-time control of recast layer formation, hardness evolution, residual stress development, and elemental redistribution. Such intelligent, data-enabled strategies will be essential for next-generation aerospace and advanced high-temperature applications.

14. Acknowledgments

The authors gratefully acknowledge the support and academic guidance provided by the Department of Mechanical Engineering, I.K. Gujral Punjab Technical University, Kapurthala, during the preparation of this review manuscript. The authors also sincerely thank the researchers and authors whose published studies contributed significantly to the development of this critical review on Wire Electrical Discharge Machining of nickel-based superalloys. No specific external funding was received for this work. The authors sincerely appreciate the time and consideration extended by the editorial board and reviewers toward this academic manuscript.

15. References

[1] L. Li, Y. B. Guo, X. T. Wei, and W. Li, "Surface Integrity Characteristics in Wire-EDM of Inconel 718 at Different Discharge Energy," *Procedia CIRP*, vol. 6, pp. 220–225, 2013, doi: 10.1016/j.procir.2013.03.046.

[2] T. R. Newton, S. N. Melkote, T. R. Watkins, R. M. Trejo, and L. Reister, "Investigation of the effect of process parameters on the formation and characteristics of recast layer in wire-EDM of Inconel 718," *Materials Science and Engineering A*, vol. 513–514, pp. 208–215, 2009, doi: 10.1016/j.msea.2009.01.061.

[3] V. S. K. Adapa, S. R. Kalidindi, and C. J. Saldana, "Insights into the gamma prime precipitation behavior during heat treatment of additively manufactured nickel-based superalloy," *Journal of Alloys and Compounds*, vol. 1012, 2025, Art. no. 178507, doi: 10.1016/j.jallcom.2025.178507.

[4] Z. Xu, G. Li, Y. Zhou, C. Guo, Y. Huang, X. Hu, X. Li, and Q. Zhu, "Tension-compression asymmetry of nickel-based superalloys: A focused review," *Journal of Alloys and*

Compounds, vol. 945, 2023, Art. no. 169313, doi: 10.1016/j.jallcom.2023.169313.

[5] A. Behera, A. K. Sahoo, and S. S. Mahapatra, "Evaluation of Physical and Thermo-Mechanical Behavior of Heat-Treated Novel Nimonic Alloy," *Journal of Materials Engineering and Performance*, vol. 34, no. 14, pp. 14757–14775, 2024, doi: 10.1007/s11665-024-10215-0.

[6] A. Pramanik, A. K. Basak, and C. Prakash, "Understanding the wire electrical discharge machining of Ti6Al4V alloy," *Heliyon*, vol. 5, no. 4, 2019, Art. no. e01473, doi: 10.1016/j.heliyon.2019.e01473.

[7] B. Ekmekci, "Residual stresses and white layer in electric discharge machining (EDM)," *Applied Surface Science*, vol. 253, no. 23, pp. 9234–9240, 2007, doi: 10.1016/j.apsusc.2007.05.078.

[8] P. V. Torres-Carrion, C. S. Gonzalez-Gonzalez, S. Aciar, and G. Rodriguez-Morales, "Methodology for systematic literature review applied to engineering and education," in 2018 IEEE Global Engineering Education Conference (EDUCON), Santa Cruz de Tenerife, Spain, Apr. 17–20, 2018, pp. 1364–1373, doi: 10.1109/educon.2018.8363388.

[9] S.Agrawal, P. Oza, R. Kakkar, S. Tanwar, V. Jetani, J. Undhad, and A. Singh, "Analysis and recommendation system-based on PRISMA checklist to write systematic review," *Assessing Writing*, vol. 61, 2024, Art. no. 100866, doi: 10.1016/j.asw.2024.100866.

[10] V. Hauk and H. Behnken, *Structural and residual stress analysis by nondestructive methods*, Amsterdam, Netherlands: Elsevier Science B.V., 1997, doi: 10.1016/b978-0-444-82476-9.x5000-2.

[11] M. E. Fitzpatrick, A. T. Fry, P. Holdway, F. A. Kandil, J. Shackleton, and L. Suominen, "Determination of residual stresses by x-ray diffraction," National Physical Laboratory, Middlesex, United Kingdom, Measurement Good Practice Guide No. 52, 2005. Accessed: Mar. 23, 2026. [Online]. Available: https://eprintspublications.npl.co.uk/2391/1/mgpg52.pdf

[12] A. Sarmast, J. Schubnell, J. Preußner, M. Hinterstein, and E. Carl, "Residual stress analysis in industrial parts: a comprehensive comparison of XRD methods," *Journal of Materials Science*, vol. 58, no. 44, pp. 16905–16929, 2023, doi: 10.1007/s10853-023-09069-z.

[13] *Standard Test Method for Microindentation Hardness of Materials*, ASTM E384-22, ASTM International, West Conshohocken, PA, USA, Nov. 2022.

[14] J. I. Goldstein, D. E. Newbury, J. R. Michael, N. W. M. Ritchie, J. H. J. Scott, and D. C. Joy, *Scanning electron microscopy and X-Ray microanalysis*, New York, NY, USA: Springer Science+Business Media LLC, 2017, doi: 10.1007/978-1-4939-6676-9.

[15] S. Suzuki, "Features of Transmission EBSD and its Application," *JOM*, vol. 65, no. 9, pp. 1254–1263, Jul. 2013, doi: 10.1007/s11837-013-0700-6.

[16] E. F. Rauch, M. Véron, S. Nicolopoulos, and D. Bultreys, "Orientation and Phase Mapping in TEM Microscopy (EBSD-TEM Like): Applications to Materials Science," *Solid State Phenomena*, vol. 186, pp. 13–15, 2012, doi: 10.4028/www.scientific.net/ssp.186.13.

[17] B. Griffiths, *Manufacturing Surface Technology: Surface Integrity & Functional Performance*, Boca Raton, FL, USA: CRC Press, 2001.

[18] I. S. Jawahir, E. Brinksmeier, R. M'Saoubi, D. K. Aspinwall, J. C. Outeiro, D. Meyer, D. Umbrello, and A. D. Jayal, "Surface integrity in material removal processes: Recent advances," *CIRP Annals*, vol. 60, no. 2, pp. 603–626, 2011, doi: 10.1016/j.cirp.2011.05.002.

[19] D. K. Aspinwall, S. L. Soo, A. E. Berrisford, and G. Walder, "Workpiece surface roughness and integrity after WEDM of Ti–6Al–4V and Inconel 718 using minimum damage generator technology," *CIRP Annals*, vol. 57, no. 1, pp. 187–190, 2008, doi: 10.1016/j.cirp.2008.03.054.

[20] M. T. Antar, S. L. Soo, D. K. Aspinwall, D. Jones, and R. Perez, "Productivity and Workpiece Surface Integrity When WEDM Aerospace Alloys Using Coated Wires," *Procedia Engineering*, vol. 19, pp. 3–8, 2011, doi: 10.1016/j.proeng.2011.11.071.

[21] L. W. Reolon, C. A. H. Laurindo, R. D. Torres, and F. L. Amorim, "WEDM performance and surface integrity of Inconel alloy IN718 with coated and uncoated wires," *The International Journal of Advanced Manufacturing Technology*, vol. 100, no. 5–8, pp. 1981–1991, 2018, doi: 10.1007/s00170-018-2828-6.

[22] P. Sharma, D. Chakradhar, and S. Narendranath, "Effect of Wire Material on Productivity and Surface Integrity of WEDM-Processed Inconel 706 for Aircraft Application," *Journal of Materials Engineering and Performance*, vol. 25, no. 9, pp. 3672–3681, 2016, doi: 10.1007/s11665-016-2216-z.

[23] P. Sharma, D. Chakradhar, and S. Narendranath, "Effect of wire diameter on surface integrity of wire electrical discharge machined Inconel 706 for gas turbine application," *Journal of Manufacturing Processes*, vol. 24, pp. 170–178, 2016, doi: 10.1016/j.jmapro.2016.09.001.

[24] L. Li, X. T. Wei, and Z. Y. Li, "Surface integrity evolution and machining efficiency analysis of W-EDM of nickel-based alloy," *Applied Surface Science*, vol. 313, pp. 138–143, 2014, doi: 10.1016/j.apsusc.2014.05.165.

[25] E. Atzeni, E. Bassoli, A. Gatto, L. Iuliano, P. Minetola, and A. Salmi, "Surface and Sub Surface Evaluation in Coated-Wire Electrical Discharge Machining (WEDM) of INCONEL® Alloy 718,"

Procedia CIRP, vol. 33, pp. 388–393, 2015, doi: 10.1016/j.procir.2015.06.089.

[26] P. M. Abhilash and D. Chakradhar, "Surface integrity comparison of wire electric discharge machined Inconel 718 surfaces at different machining stabilities," *Procedia CIRP*, vol. 87, pp. 228–233, 2020, doi: 10.1016/j.procir.2020.02.037.

[27] A. Goswami and J. Kumar, "Optimization in wire-cut EDM of Nimonic-80A using Taguchi's approach and utility concept," *Engineering Science and Technology, an International Journal*, vol. 17, no. 4, pp. 236–246, 2014, doi: 10.1016/j.jestch.2014.07.001.

[28] A. Goswami and J. Kumar, "Surface Topography and Kerf Study of Nimonic 80A Using Wire-Cut EDM," *Materials Science Forum*, vol. 808, pp. 35–41, 2014, doi: 10.4028/www.scientific.net/msf.808.35.

[29] V. Kumar, K. K. Jangra, V. Kumar, and N. Sharma, "WEDM of nickel based aerospace alloy: optimization of process parameters and modelling," *International Journal on Interactive Design and Manufacturing (IJIDeM)*, vol. 11, no. 4, pp. 917–929, 2016, doi: 10.1007/s12008-016-0298-3.

[30] C. Devanathan, Natarajan, E. Shankar, R. Giri, and K. Vigneshwaran, "An effect of process parameters during wire cut electrical discharge machining of Inconel 738," *Materials Today Proceedings*, vol. 84, pp. 83–88, 2023, doi: 10.1016/j.matpr.2023.05.148.

[31] A. G. Karthikeyan, K. Kalaiselvan, and N. Muralidharan, "CNC wire-cut EDM input variables analysis on Ni -based superalloy (MONEL K-500)," *Materials and Manufacturing Processes*, vol. 37, no. 9, pp. 1035–1044, 2021, doi: 10.1080/10426914.2021.2001522.

[32] Z. Chen, J. Moverare, R. L. Peng, and S. Johansson, "Surface Integrity and Fatigue Performance of Inconel 718 in Wire Electrical Discharge Machining," *Procedia CIRP*, vol. 45, pp. 307–310, 2016, doi: 10.1016/j.procir.2016.02.053.

[33] M. Shabgard, S. Farzaneh, and A. Gholipoor, "Investigation of the surface integrity characteristics in wire electrical discharge machining of Inconel 617," *Journal of the Brazilian Society of Mechanical Sciences and Engineering*, vol. 39, no. 3, pp. 857–864, 2016, doi: 10.1007/s40430-016-0556-0.

[34] B. Alkahlan, T. Tabbakh, A. Kurdi, A. Pramanik, and A. K. Basak, "Formation and Characterization of the Recast Layer Formed on Inconel 718 during Wire Electro Discharge Machining," *Materials*, vol. 16, no. 3, 2023, Art. no. 930, doi: 10.3390/ma16030930.

[35] P. Sharma, D. Chakradhar, and S. Narendranath, "Evaluation of WEDM performance characteristics of Inconel 706 for turbine disk application," *Materials & Design*, vol. 88, pp. 558–566, 2015, doi: 10.1016/j.matdes.2015.09.036.

[36] P. Sharma, D. Chakradhar, and N. S, "Analysis and Optimization of WEDM Performance Characteristics of Inconel 706 for Aerospace Application," *Silicon*, vol. 10, no. 3, pp. 921–930, 2017, doi: 10.1007/s12633-017-9549-6.

[37] K. Mouralova, A. Polzer, L. Benes, J. Bednar, R. Zahradnicek, T. Prokes, Z. Fiala, and J. Fries, "Machining of B1914 nickel-based superalloy using wire electrical discharge machining," *Proceedings of the Institution of Mechanical Engineers, Part E: Journal of Process Mechanical Engineering*, vol. 235, no. 6, pp. 2141–2153, 2021, doi: 10.1177/09544089211031746.

[38] S. S. Nain, D. Garg, and S. Kumar, "Modeling and optimization of process variables of wire-cut electric discharge machining of super alloy Udimet-L605," *Engineering Science and Technology, an International Journal*, vol. 20, no. 1, pp. 247–264, 2017, doi: 10.1016/j.jestch.2016.09.023.

[39] A. Mandal, A. R. Dixit, S. Chattopadhyaya, A. Paramanik, S. Hloch, and G. Królczyk, "Improvement of surface integrity of Nimonic C 263 super alloy produced by WEDM through various post-processing techniques," *The International Journal of Advanced Manufacturing Technology*, vol. 93, no. 1–4, pp. 433–443, 2017, doi: 10.1007/s00170-017-9993-x.

[40] H. Bisaria and P. Shandilya, "Experimental investigation on wire electric discharge machining (WEDM) of nimonic C-263 superalloy," *Materials and Manufacturing Processes*, vol. 34, no. 1, pp. 83–92, 2018, doi: 10.1080/10426914.2018.1532589.

[41] M. S. Rao and N. Venkaiah, "Experimental investigations on surface integrity issues of Inconel-690 during wire-cut electrical discharge machining process," *Proceedings of the Institution of Mechanical Engineers, Part B: Journal of Engineering Manufacture*, vol. 232, no. 4, pp. 731–741, 2016, doi: 10.1177/0954405416654092.

[42] R. Joy, I. V. Manoj, and S. Narendranath, "Investigation of cutting speed, recast layer and micro-hardness in angular machining using slant type taper fixture by WEDM of Hastelloy X," *Materials Today: Proceedings*, vol. 27, pp. 1943–1946, 2020, doi: 10.1016/j.matpr.2019.09.021.

[43] D Srinivasan, G Veerappan, Ravichandran M, C Anand Chairman, S Marichamy, V Mohanavel, and A Karthick, "Investigation on electric erosion behavior of nickel-based super alloy (Waspaloy: Ni, Cr, Co, Mo, Ti, Al) using response surface methodology," *Surface Topography: Metrology and Properties*, vol. 9, no. 3, 2021, Art. no. 035006, doi: 10.1088/2051-672x/ac0f33.

[44] O. C. Ozaner, G. Dursun, and G. Akbulut, "Effects of wire-EDM parameters on the surface integrity and mechanical characteristics of additively manufactured Inconel 939," *Materials*

Today Proceedings, vol. 38, pp. 1861–1865, 2021, doi: 10.1016/j.matpr.2020.08.486.

[45] V. Karthikeyan, S. Rajesh, R. G. Padmanaban, A. J. Arockiam, and S. Sundaraselvan, "Processing and Optimizing the Wire EDM Process Parameters of SLM 3D-Printed Udimet Alloy 720," *Journal of Materials Engineering and Performance*, vol. 35, no. 8, pp. 7173–7185, 2025, doi: 10.1007/s11665-025-12166-6.

[46] M. Machno, E. Franczyk, R. Bogucki, A. Matras, and W. Zębala, "A Comparative Study on the Structure and Quality of SLM and Cast AISI 316L Samples Subjected to WEDM Processing," *Materials*, vol. 15, no. 3, 2022, Art. no. 701, doi: 10.3390/ma15030701.

[47] O. Gokcekaya, A. Günen, F. Ceritbinmez, A. Bahador, T. Nakano, and M. Çetin, "Wire-EDM performance and surface integrity of Inconel 718 with unique microstructural features fabricated by laser powder bed fusion," *The International Journal of Advanced Manufacturing Technology*, vol. 130, no. 9–10, pp. 4513–4528, 2024, doi: 10.1007/s00170-023-12924-7.

[48] P. Shandilya, H. Bisaria, and P. K. Jain, "Parametric study on the recast layer during EDWC of a Ni-rich NiTi shape memory alloy," *Journal of Micromanufacturing*, vol. 1, no. 2, pp. 134–141, 2018, doi: 10.1177/2516598418766934.

[49] C. Balasubramaniyan, K. Rajkumar, and S. Santosh, "Wire-EDM machinability investigation on quaternary Ni44Ti50Cu4Zr2 shape memory alloy," *Materials and Manufacturing Processes*, vol. 36, no. 10, pp. 1161–1170, 2021, doi: 10.1080/10426914.2021.1905833.

[50] M. P. Garg, A. Kumar, and C. K. Sahu, "Mathematical modeling and analysis of WEDM machining parameters of nickel-based super alloy using response surface methodology," Sādhanā, vol. 42, no. 6, pp. 981–1005, 2017, doi: 10.1007/s12046-017-0647-3.

[51] P. S. Gowthaman and S. Jeyakumar, "A Review on machining of High Temperature Aeronautics Super-alloys using WEDM," *Materials Today: Proceedings*, vol. 18, pp. 4782–4791, 2019, doi: 10.1016/j.matpr.2019.07.466.

[52] Sudhir, A. K. Sehgal, and S. S. Nain, "Machine learning algorithms evaluation and optimization of WEDM of nickel based super alloy: A review," *Materials Today: Proceedings*, vol. 50, pp. 1793–1798, 2022, doi: 10.1016/j.matpr.2021.09.202.

[53] A. Polzer, K. Mouralova, L. Benes, R. Zahradnicek, and J. Fries, "Comparison of machinability of nickel alloys using WEDM," *Proceedings of the Institution of Mechanical Engineers, Part B: Journal of Engineering Manufacture*, vol. 236, no. 9, pp. 1268–1281, 2022, doi: 10.1177/09544054221075876.

[54] S. Biswas, A. R. Paul, A. R. Dhar, Y. Singh, and M. Mukherjee, "Multi-material modeling for wire electro-discharge machining of Ni-based superalloys using hybrid neural network and stochastic optimization techniques," *CIRP Journal of Manufacturing Science and Technology*, vol. 41, pp. 350–364, 2023, doi: 10.1016/j.cirpj.2022.12.005.

[55] A. G. Joshi, R. Suresh, M. Manjaiah, and A. Soni, "Parametric optimization of output responses in wire electrical discharge machining of inconel 718: An integrated TOPSIS-multi-objective ant-lion approach," *Materialwissenschaft und Werkstofftechnik*, vol. 57, no. 7, pp. 708–722, 2026, doi: 10.1002/mawe.70148.

[56] P. Kumar, M. Gupta, and V. Kumar, "Surface integrity analysis of WEDMed specimen of Inconel 825 superalloy," *International Journal of Data and Network Science*, pp. 79–88, 2018, doi: 10.5267/j.ijdns.2018.8.001.

[57] P. M. Abhilash and D. Chakradhar, "Prediction and analysis of process failures by ANN classification during wire-EDM of Inconel 718," *Advances in Manufacturing*, vol. 8, no. 4, pp. 519–536, 2020, doi: 10.1007/s40436-020-00327-w.

[58] D. Oniszczuk-Świercz, R. Świercz, and Š. Michna, "Evaluation of Prediction Models of the Microwire EDM Process of Inconel 718 Using ANN and RSM methods," *Materials*, vol. 15, no. 23, 2022, Art. no. 8317, doi: 10.3390/ma15238317.

[59] A. Sharma, A. Thakur, and J. P. Misra, "Machine learning-based predictive model for wire electric discharge machining of Incoloy 800H," *Proceedings of the Institution of Mechanical Engineers, Part E: Journal of Process Mechanical Engineering*, 2025, doi: 10.1177/09544089251377617.

[60] U. Küpper, E. Tchoupe, A. Klink, and T. Bergs, "Prediction of Geometrical Accuracy in Wire EDM by Analyzing Process Data," *Procedia CIRP*, vol. 113, pp. 23–28, 2022, doi: 10.1016/j.procir.2022.09.114.

[61] A. R. Lakkundi and V. N. Kulkarni, "Physics-informed hybrid digital twin for real-time multi-sensor intelligence and adaptive control in wire electrical discharge machining," *Applied Soft Computing*, vol. 198, 2026, Art. no. 115267, doi: 10.1016/j.asoc.2026.115267.

[62] P. M. Abhilash and D. Chakradhar, "Failure detection and control for wire EDM process using multiple sensors," *CIRP Journal of Manufacturing Science and Technology*, vol. 33, pp. 315–326, 2021, doi: 10.1016/j.cirpj.2021.04.009.

[63] S. N. Grigoriev, M. P. Kozochkin, V. D. Gurin, A. P. Malakhinsky, A. N. Porvatov, and Y. A. Melnik, "Display of WEDM Quality Indicators of Heat-Resistant Alloy Processing in Acoustic Emission Parameters," *Sensors*, vol. 23, no. 19, 2023, Art. no. 8288, doi: 10.3390/s23198288.

[64] W. Ming, X. Guo, G. Zhang, S. Hu, Z. Liu, Z. Xie, S. Zhang, and L. Duan, "Optimization of process parameters and performance for machining

Inconel 718 in renewable dielectrics," *Alexandria Engineering Journal*, vol. 79, pp. 164–179, 2023, doi: 10.1016/j.aej.2023.07.075.

[65] P. M. Abhilash and D. Chakradhar, "Effect of wire material and discharge energy on productivity and surface integrity of WEDM-processed Inconel 718," *Advances in Materials and Processing Technologies*, vol. 8, no. 4, pp. 4698–4719, 2022, doi: 10.1080/2374068x.2022.2079590.

[66] Y. Wang, J. Miao, S. Chen, R. Jin, W. Xiong, and Y. Chen, "Study on the surface integrity in ultrasonic vibration and magnetic field complex assisted low speed WEDM under different magnetic field coupling," *Journal of Manufacturing Processes*, vol. 90, pp. 257–273, 2023, doi: 10.1016/j.jmapro.2023.01.083.